

5.3A A COMPUTATIONAL FLUID DYNAMICS METHOD FOR RADIOSONDE SOLAR RADIATION ERROR CORRECTION

Qingquan Liu^{1*}, Wei Dai², Jie Yang²

1. School of Electronic and Information Engineering, Nanjing University of Information Science and Technology, Nanjing, China
2. Key Laboratory for Aerosol-Cloud-Precipitation of China Meteorological Administration, Nanjing University of Information Science and Technology, Nanjing, China

1. INTRODUCTION

Air temperature of high altitude is considered as an important factor in both weather forecast and climate change research. Due to the increasing amount of attention that has been focused on numerical weather forecast and climate change research, it is desired that the accuracy of upper air temperature measurement can be reduced to 0.1 K. During the day, direct solar radiation produces an additional and considerably larger error on the temperature measurement, which has become the bottleneck when improving the accuracy of upper air radiosonde temperature sensors. Currently, the experiments and theoretical calculations are the methods used to study the correction of solar radiation heating error. Dominique (2003) built a simple low-pressure radiation wind tunnel platform for radiation error research. However, the measurement results are obtained by this simple experiment platform are not representative of the real sounding data. Based on the previous work, James (1990, 1995) built a simplified model of rod thermistor for analyzing solar radiation error. But the Reynolds number in the formula can only be obtained by empirical estimation. Rolf (2013) set up the radiation experiment platform for measuring with thermal radiation errors of the very

thin thermocouple of the Meteolabor SRS-C34 radiosonde on the same flight, simultaneously under sun-shaded and unshaded conditions. However, the wind pulsation may change the sun-shaded condition of the thermocouple sensor, which influences the accuracy of temperature measurement. The World Meteorological Organization (1996) has provided some correction ranges for solar radiation errors, without any precise and quantitative data. Due to the environmental constraints of upper air sounding, it is difficult to achieve a high precision. So these conventional techniques are essentially unable to meet the needs of numerical weather prediction and climate change research.

Based on existing research and theory, this paper proposes a new method of numerical simulation to improve the measurement accuracy of the temperature sensor and make up for the shortages of the traditional solutions. A computational fluid dynamics (CFD) method can efficiently solve computational problems of complex flow and heat transfer in various fields, and it is employed to simulate whole process of the sounding temperature sensor from sea level to 32 km altitude. On the basis, aiming at various air thermal conductivities and solar elevation angles, that affect measurement precision are analyzed. The modeling results of this method have a potential to scale the solar radiation errors down to roughly 0.1 K magnitude.

2. CFD modeling of sounding temperature sensor

2.1 Physical model

Bian (2011) and Kentaro (2010) mention that the

* Corresponding author address: Qingquan Liu, School of Electronic and Information Engineering, Nanjing University of Information Science and Technology, 219 Ningliu Road, Nanjing City, Jiangsu Province, China, 210044; e-mail: andyucd@163.com.

bead thermistor is an important measurement component in a radiosonde system. It is widely used to measurement atmospheric temperature from the sea level to an altitude of approximately 32 km height in the arena of meteorological observation. It has the advantages of small size, high sensitivity and the ability of heat. Its 2-D drawing and feature size are summerized in Fig.1.

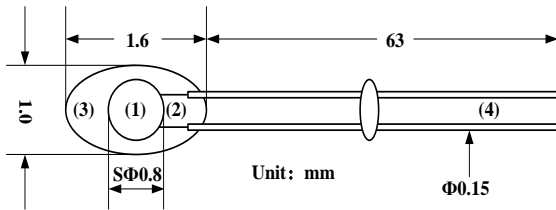


Figure 1. 2-D drawing and feature size of the bead thermistor
(1.Resistor body, 2.Electrodes, 3.Insulating layer, 4.Lead)

The bead thermistor is composed of a resistor body, a pair of electrodes, an insulating layer and a pair of leads. The material properties of the components are listed in Table 1.

Table 1. The physical parameters of the bead thermistor

| Material: components | Thermal conductivity w/(m k) |
|-------------------------|---------------------------------|
| Epoxy: insulating layer | 0.2 |
| Ceramics: resistor body | 35 |
| Platinum: Lead | 73 |

The temperature sensor studied in this paper ascends from sea level to approximately 32 km altitude, and the atmospheric pressure decreases over three orders of magnitude in the process, which affects the convective heat transfer of the temperature sensor significantly. According to COESA(1976) published the U.S. standard atmosphere in 1976, the relationship

between the air pressure and the altitude is given. The air pressure at various elevations is obtained, such as shown in Fig. 2.

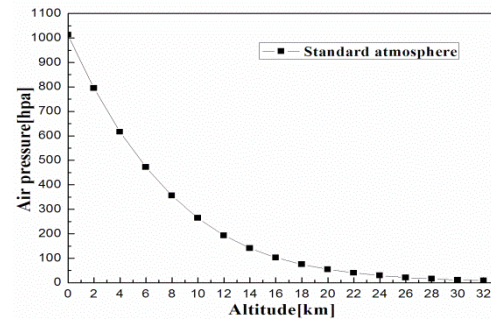


Figure 2. The relationship between air pressure and altitude

The bead thermistor working at different altitudes are exposure to complicated thermal environment. By considering all the possible heat transfer types, thermal environment of the bead thermistor at rising condition was diagrammed in Fig. 3. The objects that will influence thermal performance of the bead thermistor. In detail, the external thermal fluxes include the direct solar radiation and the convective heat flux between the bead thermistor and the air.

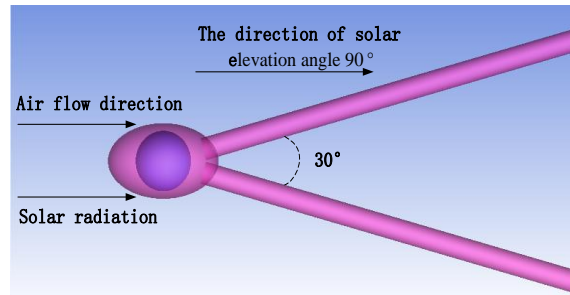


Figure 3. Thermal environment of the bead thermistor

2.2 Control equations

The basic control equations of CFD numerical simulation are composed of mass conservation equation, momentum conservation equation and energy conservation equations.

The formula of mass conservation equation is:

$$\frac{\partial \rho}{\partial t} + \frac{\partial \rho u}{\partial x} + \frac{\partial \rho v}{\partial y} + \frac{\partial \rho w}{\partial z} = 0 \quad (1)$$

Where ρ in Eq. (1) represents density, t represents time, u, v, w represents the component of velocity vectors in the X, Y, Z axis direction, respectively.

The formula of momentum conservation equation can be expressed as:

$$\frac{\partial(\rho u)}{\partial t} + \frac{\partial(\rho uu)}{\partial x} + \frac{\partial(\rho uv)}{\partial y} + \frac{\partial(\rho uw)}{\partial z} = -\frac{\partial p}{\partial x} + \frac{\partial \tau_{xx}}{\partial x} + \frac{\partial \tau_{yx}}{\partial y} + \frac{\partial \tau_{zx}}{\partial z} + F_x \quad (2)$$

$$\frac{\partial(\rho v)}{\partial t} + \frac{\partial(\rho vu)}{\partial x} + \frac{\partial(\rho vv)}{\partial y} + \frac{\partial(\rho vw)}{\partial z} = -\frac{\partial p}{\partial y} + \frac{\partial \tau_{xy}}{\partial x} + \frac{\partial \tau_{yy}}{\partial y} + \frac{\partial \tau_{zy}}{\partial z} + F_y \quad (3)$$

$$\frac{\partial(\rho w)}{\partial t} + \frac{\partial(\rho wu)}{\partial x} + \frac{\partial(\rho wv)}{\partial y} + \frac{\partial(\rho ww)}{\partial z} = -\frac{\partial p}{\partial z} + \frac{\partial \tau_{xz}}{\partial x} + \frac{\partial \tau_{yz}}{\partial y} + \frac{\partial \tau_{zz}}{\partial z} + F_z \quad (4)$$

Where p in Eq. (2 ~ 4) represents the pressure of the micro unit, $\tau_{xx}, \tau_{xy}, \tau_{xz}$ represents the component of the viscous stress the molecular viscous effects in infinitesimal surface, respectively, F_x, F_y, F_z represents the volume forces of the micro unit.

The formula of energy conservation equation is given by:

$$\frac{\partial(\rho T)}{\partial t} + \text{div}(\rho u T) = \text{div}\left(\frac{\lambda}{c_p} \text{grad} T\right) - \frac{\partial p}{\partial x} + S_T \quad (5)$$

Where c_p in Eq. (5) represents specific heat, T represents thermodynamic temperature, λ represents thermal conductivity of the fluid, S_T represents source term.

2.3 Meshing

The bead thermistor has an irregular geometric shape. Hence it is necessary to use strong adaptive unstructured grid. In order to accurately capture the physical phenomena in the boundary layer, a boundary layer grid technology is implemented. It can help to improve the calculation accuracy of the simulation. The entire mesh of the bead thermistor model and the peripheral air domain is shown in Fig.4.

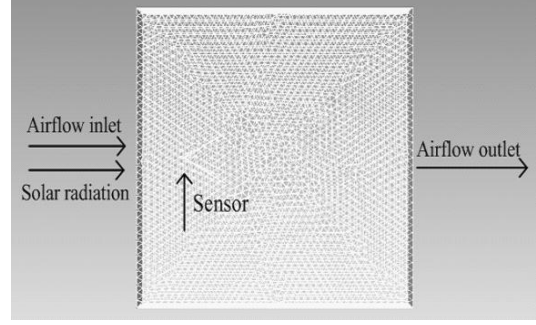


Figure 4. The grids of the bead thermistor model and peripheral air domain

2.4 Boundary conditions and calculation methods

Boundary conditions are the conditions on the boundary of the fluid motion control equation that should be satisfied. These settings will have a remarkable impact on solution results. The boundary conditions are set as follows.

- (1) A velocity inlet boundary condition should be used for air inlet wall, and it applies to incompressible flow problems.
- (2) The air outlet wall features a pressure outlet boundary condition, where the outlet pressure is set to 0 Pa.
- (3) Slip wall boundary conditions is applied for the other walls with a wall movement speed of 6 m/s.

Jeffrey (2008) proposed that, while dealing with low-speed airflow slower than 100 m/s, the compressibility effects can be ignored. Since the relative airflow velocity is 6 m/s, the ambient air can be regarded as incompressible. The pressure-based solver is employed due to the attribution that it mainly deals with low-speed incompressible flow. Energy equations are required for the model that involved radiative and convective heat transfer and thermal conduction. Control equations are discretized by a finite volume method, in which discrete format uses second-order differential format. In the Momentum equation, under-relaxation technique should be used to prevent divergence in the iterative process. Semi-Implicit Method for Pressure-Linked Equation (SIMPLE) is utilized for the pressure and speed decoupling. The

solution of momentum, energy and turbulence parameters requires the use of first-order upwind scheme for convergence of the calculation results and then the use of the second-order upwind scheme to improve the accuracy of the calculated results.

3. Numerical simulation results and analysis

In order to reveal the relationship between the air thermal conductivities, the solar elevation angles and the solar radiation errors, a surface coating reflectivity of 70 %, a resistor body diameter size of 0.8 mm and a solar direct radiation of 1200 w/m^2 have been used, when the model is built. To take various air thermal conductivities and solar elevation angles into consideration, the range of air thermal conductivity is from 0.018 to 0.024 w/(m k) in our models, where the step of the change is 0.001 w/(m k). And the range of solar elevation angle is from 0 to 90° in our models, where the step of the change is 30° . The results of the solar radiation errors are obtained in post processing. Fig. 5 displays the data relationships between the air thermal conductivities, the solar elevation angles and the solar radiation errors from sea level to 32 km altitude.

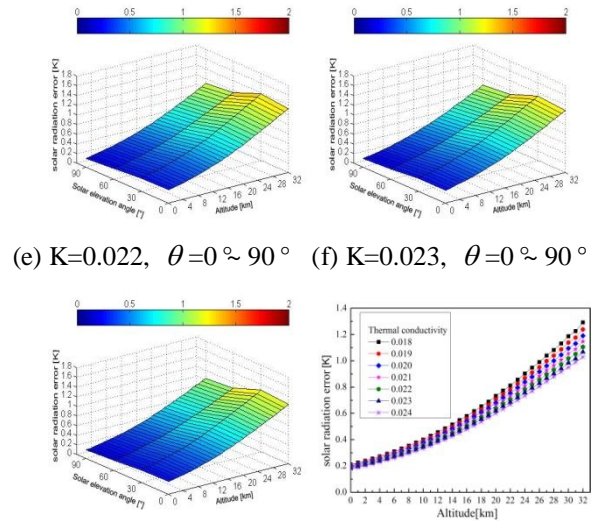
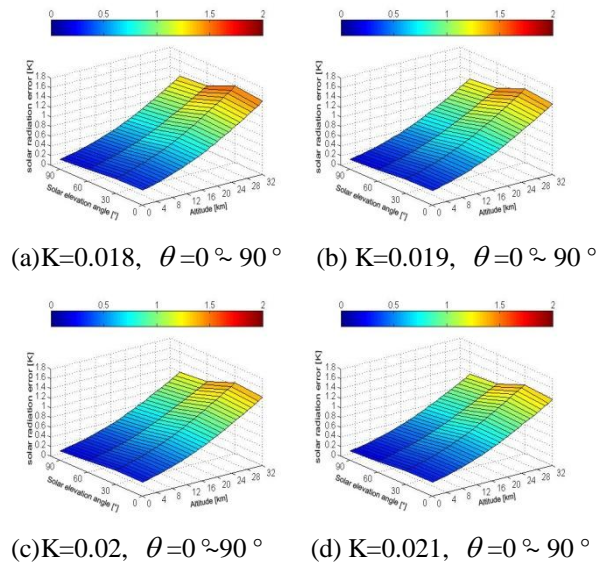


Figure 5. The discrepancy of the solar radiation errors of the different air thermal conductivities and solar elevation angles

The plots in Fig. 5 imply that, under different air thermal conductivities and solar elevation angles, the data relationship of the solar radiation error and the altitude is approximately an exponential function. The solar radiation error monotonically increases with altitude. At sea level or near sea level, the discrepancy of the solar radiation error resulted from different air thermal conductivities and solar elevation angles can be ignored. As the altitude increases, this discrepancy increases rapidly. Fig. 5 (a) ~ (g) shows that the solar radiation error can be partially compromised with increasing solar elevation angle. As the altitude is up to 32 km, the discrepancy of the radiation error is up to 0.2 K between 0° and 90° . When the solar elevation angle is 90° , the solar radiation error of the bead thermistor model is minimized. It is clear that the solar radiation error monotonically increases with altitude in Fig.5 (h). As the altitude is up to 32 km, the discrepancy of the radiation error is up to 0.3 K, while the air thermal conductivity is between 0.018 and 0.024 w/(m k). When the air thermal conductivity is 0.18 w/ (m k), the solar radiation error of the bead thermistor model is minimized.

4. Conclusion

This paper uses a CFD method to perform numerical analysis on the bead thermistor in various air pressures, air thermal conductivities and solar elevation angles. It demonstrates the potential of this CFD method that can be used to improve the accuracy of radiation error correction. The following conclusions can be obtained.

(1) The heating effect of the solar radiation on the bead thermistor can cause significant temperature measurement error. Therefore, the error needs to be corrected.

(2) When solar elevation angle is 90° , the solar radiation induces less error. This radiation direction is preferred in future radiosonde sensor applications.

(3) The change of the air thermal conductivity can influence the observation accuracy of the bead thermistor in the upper air. Therefore, the change of the air thermal conductivity should not be neglected.

5. Acknowledgments

The project is supported by China Meteorology Administration (CMA) and China Ministry of Science and Technology (MOST) under contracts GYHY200906037 and GYHY201106048. The work is also sponsored by National Natural Science Foundations of China (NSFC) under contracts 41075026 and 41275042. This research is also funded by Advantage Subject Construction Project of Jiangsu Province, China (the project of sensor networks and modern meteorological equipment) and by the Science and Technology Supported Program Key Project of Jiangsu Province, China under contract BE2011006.

6. References

Ruffieux, D., Joss, J., 2003: Influence of Radiation on the Temperature Sensor mounted on the Swiss Radiosonde. *Journal of Atmospheric and Oceanic Technology.*, 11, 1576-1582.

Luers, J. K., 1990: Estimating the Temperature Error of

the Radiosonde Rod Thermistor under different Environments. *Journal of Atmospheric and Oceanic Technology.*, 7, 882-895.

Luers, J. K., Eskridge, R. E., 1995: Temperature Corrections for the VIZ and Vaisala Radiosondes. *Journal of Atmospheric and Oceanic Technology.*, 6, 1241-1253.

Philipona, R., Kräuchi, A., Romanens, G., Levrat, G., Ruppert, P., Brocard, E., Jeannet, P., Ruffieux, D., Calpini B., 2013: Solar and Thermal Radiation Errors on Upper-Air Radiosonde Temperature Measurements. *Journal of Atmospheric and Oceanic Technology.*, 10, 2382-2393.

WMO, 1996: Guide to Meteorological Instruments and Methods of Observation, Secretariat of WMO, Geneva.

Jianchun, B., Hongbin, C., Holger, V., Yunjun, D., Yuejian, X., Daren, L., 2011: Intercomparison of Humidity and Temperature Sensors: GTS1, Vaisala RS80, and CFH. *Journal of Advances In Atmospheric Sciences.*, 1, 139-146.

Shimizu, K., Hasebe, F., 2010: Fast-response High-resolution Temperature Sonde aimed at Contamination-free Profile Observations. *Journal of Atmospheric Measurement Techniques.*, 6, 1673-1681.

COESA, 1976: U. S. Standard Atmosphere. U. S. Government Printing Office, USA.

Housman, J., Kiris, C., Hafez, M., 2008: Preconditioned Methods for Simulations of Low Speed Gas Compressible Flows, *Journal of Computers and Fluids.*, 7, 1411-1423.